processes

MDPI

Article

Thermal Stability Evaluation of T152 Emulsifier on the Modification Influence of Fireworks Propellant

He Wu, Na Yang, Yan Tang, Jun-Cheng Jiang * and An-Chi Huang *

School of Safety Science and Engineering, Changzhou University, Changzhou 213164, China
* Correspondence: jiangjc@cczu.edu.cn (J.-C.J.); huangac@cczu.edu.cn (A.-C.H.)

Abstract: High-energy substances like effect propellant and propellant are used in fireworks. In the process of manufacture, transportation, and use, heat can easily get out of control. The emulsifier polyisobutene succinimide (T152) is frequently used to emulsify explosives. Given the thermal safety of the propellant in fireworks, this paper used the emulsifier T152 to emulsify the propellant. Thermogravimetric Fourier-transform infrared spectrometry and differential scanning calorimetry were used to analyze and test the propellant. In addition, several methods of thermokinetic calculation were used to calculate thermal stability. The thermal stability of the propellant before and after adding T152 was compared and analyzed. The test results indicate that the apparent activation energy of the propellant increases with the addition of T152. The emulsifier improved the thermal stability of the propellant. The research results can provide relevant data and suggestions for the thermal reaction of pyrotechnic propellants, thereby reducing the potential risks of the fireworks industry.

Keywords: thermal hazard; TG-FTIR; emulsified propellant; fireworks

Citation: Wu, H.; Yang, N.; Tang, Y.; Jiang, J.-C.; Huang, A.-C. Thermal Stability Evaluation of T152 Emulsifier on the Modification Influence of Fireworks Propellant. *Processes* **2022**, *10*, 1606. https://doi.org/10.3390/pr10081606

Academic Editors: Xu Chen, Weiyi Xing and Shouwen Shi

Received: 18 July 2022
Accepted: 11 August 2022
Published: 13 August 2022

1. Introduction

Fireworks have long been a widely used commodity around the world. They are highly ornamental, carry different cultural connotations, and play an irreplaceable role [1]. However, their safety problems cannot be underestimated as a high risk factor [2]. The production process of fireworks is complicated, and many uncontrollable factors make the production process very dangerous. In the production process of finished products, semi-finished products, and raw materials, fireworks have flammable and explosive characteristics. Therefore, the production process can easily lead to fire and explosion accidents [3].

The uncontrolled usage of fireworks has resulted in numerous fatalities in recent years. For instance, on 4 December 2019, an explosion accident at Bixi Fireworks Manufacturing Co., Ltd. in Liuyang City, Hunan Province, China, resulted in 13 fatalities and 13 injuries, as well as a direct economic loss of 19.446 million yuan. Similarly, in June 2018, a fireworks warehouse explosion in Tultepec, Mexico, resulted in at least 24 fatalities and dozens of injuries. Finally, on 5 February 2019, 5 people were killed in a major fireworks accident in Liuzhou, China.The heavy casualties caused by these accidents demonstrate the potential dangers of fireworks [4,5].

Propellant is a typical energetic material and constitutes the main part of fireworks and firecrackers [6]. The presence of high-energy materials makes fireworks flammable and explosive. In its production, transportation, and storage, if it is affected by external energy, it will lead to combustion and explosion accidents [7]. The pyrotechnic medicine in fireworks is mainly composed of reducing agents, oxidants, and adhesives [8]. The response mode of a firework determines its safety during production and use. Statistics show that of all forms of energy stimulation, heat is the most common cause of accidents. Therefore, the essence of firework accidents lies in the firework system's thermal imbalance [9,10]. A scientific and effective thermal safety evaluation method for fireworks can prevent accidents, reduce economic and property losses and casualties, and promote the development of the fireworks industry [11]. Therefore, it is essential to study the thermal safety of fireworks.

Emulsifiers are a crucial component of emulsified explosives, and their chemical properties are closely related to their explosive properties and stability [12,13]. Polyisobutene succinimide (T152) is a high-viscosity polymer emulsifier that has a cross-linking solid effect on droplets and can adsorb on the oil–water interface [14]. T152 emulsifier is non-toxic and non-irritating and is an ideal emulsifier for the production of emulsion explosives. In addition, T152 also has the advantage of good storage stability, so this paper selects T152 emulsifier as the research object. In this experiment, the T152 emulsifier was added to fireworks propellant to assess its impact on the thermal stability.

Based on thermal reaction kinetics, this study conducted experiments on fireworks launchers and emulsified launchers using thermal analysis instruments such as thermogravimetric Fourier-transform infrared spectrometry (TG-FTIR) and differential scanning calorimetry (DSC). The investigation obtained the thermal parameters of the fireworks propellant (PA) to evaluate the thermal safety of fireworks and firecrackers. The main research content includes two aspects: the thermal stability of fireworks propellants and emulsified propellants (PA-T152). The evolution of gaseous products during combustion was analyzed by infrared spectroscopy, thermokinetic reactions were modeled, and simulation calculations were performed. This practical study can provide reference data for accident prevention in the fireworks propellant context. If produced, the new propellant prepared in this study can reduce the risk of fireworks propellant during production and storage, which is very important.

2. Experimental and Methods

2.1. Sample

The primary experimental samples studied in this paper are from multitube fireworks products purchased from Tianjiao fireworks factory (Liuyang, Hunan, China). Their internal structure is diagrammed in Figure 1.

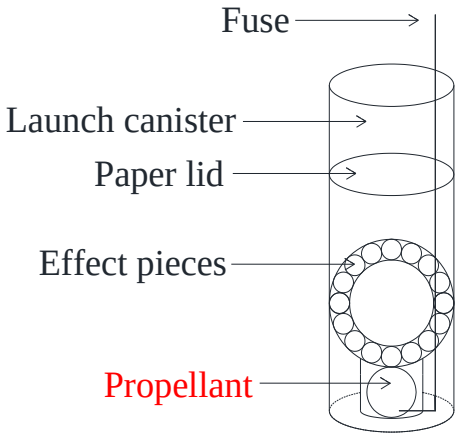

Figure 1. Schematic diagram of fireworks section.

The main chemical involved in this experiment is polyisobutene succinimide (T152), purchased from Wuxi Southern Petroleum Additives Co., Ltd. (Wuxi, Jiangsu, China). Its physical properties include being a brown transparent viscous liquid with dispersible SDT > 55 [15]. T152 emulsifier has good low-temperature dispersion performance and certain high-temperature detergency. Furthermore, it also has the characteristics of good oil solubility, is insoluble in water, is slightly soluble in ethanol, and is non-volatile. Its relative molecular weight is around 800–5000 [16]. Its molecular structural formula is shown in Figure 2.

In the experiment, we ground the PA sample into a powder and dried it in a desiccator for 8 h. According to the physical and chemical properties of the PA, the drying temperature was set to 80 °C, and the vacuum degree was 0. Subsequently, the T152

emulsifier and propellant samples were mixed and stirred according to a proportion of 30% for thermogravimetric experiment.

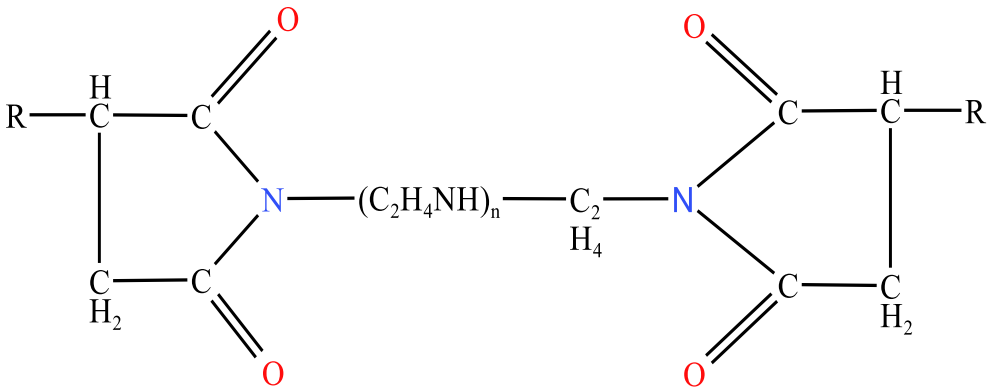

Figure 2. Molecular structural formula of polyisobutene succinimide (T152).

The main experimental method of this experiment was the control experiment method. PA was used as a blank control, as a comparison standard, and PA-T152 was used as an experimental group to compare with PA. Except for the addition of T152, the other conditions of the two samples were the same. The experiment was set up as five groups of experiments with heating rates of 2.0, 4.0, 6.0, 8.0, and 10.0 °C/min, respectively. In order to avoid experimental errors and ensure the same experimental conditions, each group of experiments was repeated three times or more. The measurement procedures for the experiments were all the same.

2.2. Thermogravimetric Fourier-Transform Infrared Spectrometry (TG-FTIR)

Thermogravimetric analysis is a technique for determining the relationship between the quality change of a substance and temperature (or time) over a temperature range controlled by a specified program [17,18]. We can analyze experimental curves to learn about changes in the quality of the sample, the thermal stability of the sample, and the products of thermal decomposition. Fourier-transform infrared spectrometric analysis is an essential modern sample analysis method, which can identify the content of functional groups in the sample, widely used in the qualitative and quantitative analysis of all material samples [19,20]. The experiment to analyze the effect of the T152 emulsifier on PA used TG-IR (Nicolet iS20) produced by Thermo Fisher Scientific and TGA (TGA 2) produced by Mettler Toledo of Switzerland. The data acquisition frequency of FTIR was 5 s, the wave number range was 4000–400 cm^{-1}, and the resolution was 1 cm^{-1}. The experiment was carried out in a nitrogen atmosphere, and the net quality control of the sample was 1.80 ± 0.5 mg. Because the PA is high risk, the experimental dosage was very low to ensure the safety of the experiment. The heating range was set to 30.0–600.0 °C. The heating rate (β) of the experimental samples was set to 2.0, 4.0, 6.0, 8.0, and 10.0 °C/min.

2.3. Differential Scanning Calorimetry (DSC)

DSC is a thermal analysis technique that records the power difference between samples, references, and temperature (or time) under procedural temperature control. It is one of the most widely used thermal analysis techniques in thermogravimetric research [21,22]. The instrument used in this experiment was the DSC 821^e (Mettler TA8000 system). Given that PA samples release much heat during the heating investigation, the experiment was performed in a golden crucible with a capacity of 40 μL. The temperature rise range of the experimental sample was 30.0–400.0 °C, and the β was consistent with the TGA experiment. When weighing propellants and emulsified propellant samples, the net quality control was 2.0 ± 0.5 mg. The entire measurement process took place in an air atmosphere.

2.4. Thermokinetic Analysis Methods

2.4.1. Kissinger Method

The Kissinger method, also known as the maximum method, is one of the basic methods for calculating the apparent activation energy (E_a) of composite materials. According to the Arrhenius kinetic equations, it can be obtained as [23,24]:

$$\frac{d\alpha}{dt} = k(T)f(\alpha) = \left(A^{-\frac{E_a}{RT}}\right)f(\alpha) = A^{-\frac{E_a}{RT}}(1-\alpha)^n \quad (1)$$

where $k(T)$ is the reaction rate constant, T is the absolute temperature (K), $f(\alpha)$ is the reaction function, and α is the conversion rate. A is the pre-exponential factor (s^{-1}), and E_a is the apparent activation energy. R represents the universal gas constant (8.314 J mol^{-1} K^{-1}) [25], while $(1-\alpha)^n = f(\alpha)$ represents a differential form of a dynamic function.

When $T = T_p$, that is, when the temperature reaches the maximum value, $d^2\alpha/dt^2 = 0$. By differentiating both sides of Equation (1) and substituting $d^2\alpha/dt^2 = 0$, we can obtain:

$$\frac{d^2\alpha}{d^2t} = \frac{d\alpha}{dt}\left[\frac{E_a\beta}{RT_p{}^2} - A^{-\frac{E_a}{RT}}n(1-\alpha)^{n-1}\right] = 0 \quad (2)$$

That is:

$$\frac{E_a\beta}{RT_p{}^2} = A^{-\frac{E_a}{RT}}n(1-\alpha)^{n-1} \quad (3)$$

Kissinger considered that $n(1-\alpha)^{n-1}$ is independent of β [26]. Therefore, the logarithm of Equation (3) is taken to obtain:

$$\ln\left(\frac{\beta}{T_p{}^2}\right) = \ln\left(\frac{AR}{E_a}\right) - \frac{E_a}{RT_p} \quad (4)$$

Different β were connected to a straight line. The values of A and E_a can be determined by the intercept and slope of the line, respectively [27].

2.4.2. Friedman Method

The Friedman method is also a kinetic analysis method based on the Arrhenius equation. Its differential equal conversion equation is [28]:

$$\ln\left(\frac{d\alpha}{dt}\right)_\alpha = \ln[Af(\alpha)] - \frac{E_a}{RT} \quad (5)$$

where $d\alpha/dt$ is the reaction rate (s^{-1}).

2.4.3. KAS Method

The KAS (Kissinger–Akahira–Sunose) method is similar to the Kissinger method [29], but the results are more comprehensive. As shown in Equation (6), the KAS equation is [30]:

$$\ln\left(\frac{\beta}{T^2}\right) = \ln\left[\frac{AR}{E_aG(\alpha)}\right] - \frac{E_a}{RT} \quad (6)$$

Slightly different from the Kissinger method, the absolute temperature T(K) corresponding to different α values is also different. $G(\alpha)$ is the integral form of a dynamic mechanism function.

2.4.4. FWO Method

For different β, we can use FWO (Flynn–Wall–Ozawa) method for thermokinetic calculation; its equation is as follows [31]:

$$\ln \beta = \ln\left[\frac{AE_a}{RG(\alpha)}\right] - 2.315 - 0.4567\frac{E_a}{RT} \quad (7)$$

E_a was obtained from the slope of two lines, lnβ and $1/T$.

2.4.5. Vyazovkin Method

Vyazovkin proposed a model-free dynamics integration equation that is a function of temperature change under the same α [32]. Its formula is as follows [33]:

$$-\ln t_{\alpha,t} = \ln\left[\frac{A_a}{g(\alpha)}\right] - \frac{E_a}{RT} \quad (8)$$

where $t_{\alpha,t}$ is the time it takes to achieve different conversion rates.

2.4.6. Starink Method

The Starink method has a great deal of practical experience and exceptional accuracy. Starink conducted a summary analysis on the predecessor method and proposed a new equation [34]:

$$\ln\left(\frac{\beta}{T^{1.8}}\right) = C_s - 1.0037\frac{E_a}{RT} \quad (9)$$

where C_s in the equation is a constant.

3. Results and Discussion

3.1. Thermal Parameters of PA and PA-T152

3.1.1. Thermogravimetric Analysis Results

The TG and DTG curves of PA and PA-T152 at different β are shown in Figures 3 and 4. The mass loss process of pure fireworks propellant can be divided into two stages. It can be seen from the figure that $T_{0,s1}$ of the PA in the first stage occurs at 82.8–100.7 °C. The $T_{0,s2}$ of the second-stage PA occurs in the temperature range of 233.8–269.2 °C. The reaction time of the thermal mass loss of PA reduces with the growth of β because the mass loss in both stages increases with the increase of β value. The thermal breakdown of components like sulfur in the PA may be the cause of the mass loss in the first step of the diagram. The mass loss in the second stage may be due to thermal decomposition. Figure 4 also shows the results of the mass loss derivative of fireworks propellant as a function of temperature at different β.

As seen in Figures 3 and 4, the quality loss process of PA-T152 is also in two stages. Among them, the $T_{0,s1}$ of the first stage occurs between 90.1–114.4 °C, and the mass loss $T_{0,s2}$ of PA-T152 in the second stage is 251.7–287.2 °C. Compared with the pure propellant mentioned above, the T_0 of PA-T152 is significantly higher, indicating that the thermal stability of PA-T152 is higher than that of pure propellant. It may be that the presence of T152 leads to a decrease in the decomposition rate of the PA. The thermogravimetric loss comparison data of PA and PA-T152 are presented in Table 1 and Figure 5.

Table 1. Thermogravimetric loss data for PA and PA-T152.

Sample β (°C/min)	Mass (mg)	PA			PA-T152		
		$T_{0,s1}$ (°C)	$T_{0,s2}$ (°C)	Maximum DTG (%/°C)	$T_{0,s1}$ (°C)	$T_{0,s2}$ (°C)	Maximum DTG (%/°C)
2.0	1.80 ± 0.5	82.8	233.8	0.66	90.1	251.7	0.61
4.0		94.9	241.1	0.65	110.7	274.6	0.59
6.0		95.2	261.2	0.60	118.1	280.4	0.56
8.0		96.8	268.3	0.56	119.1	285.4	0.48
10.0		100.7	269.2	0.47	114.4	287.2	0.44

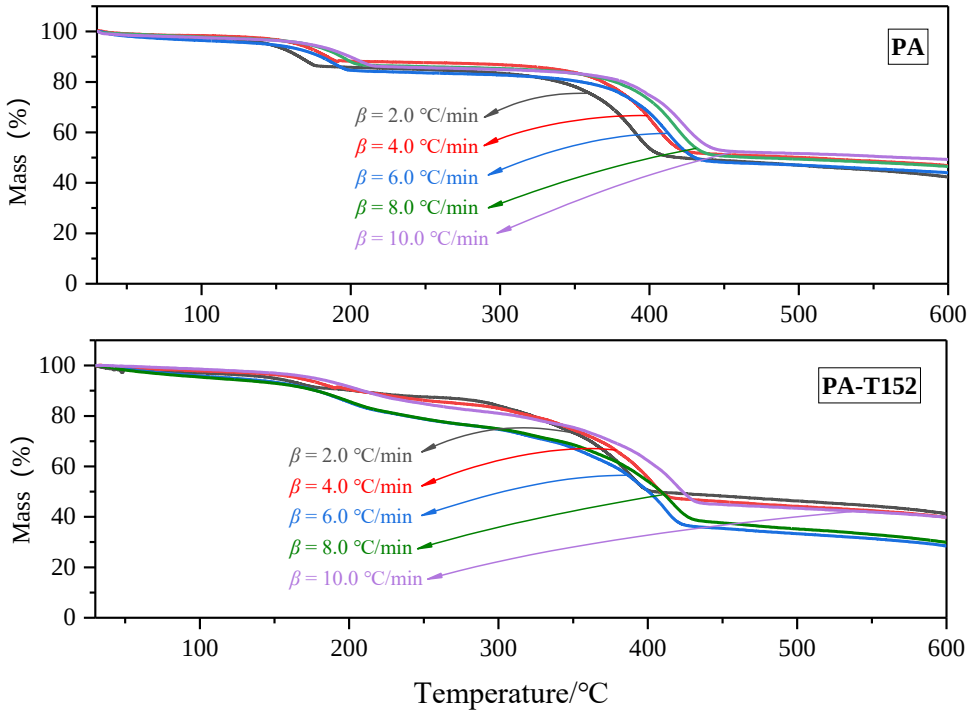

Figure 3. TG curves of PA and PA-T152 at different β.

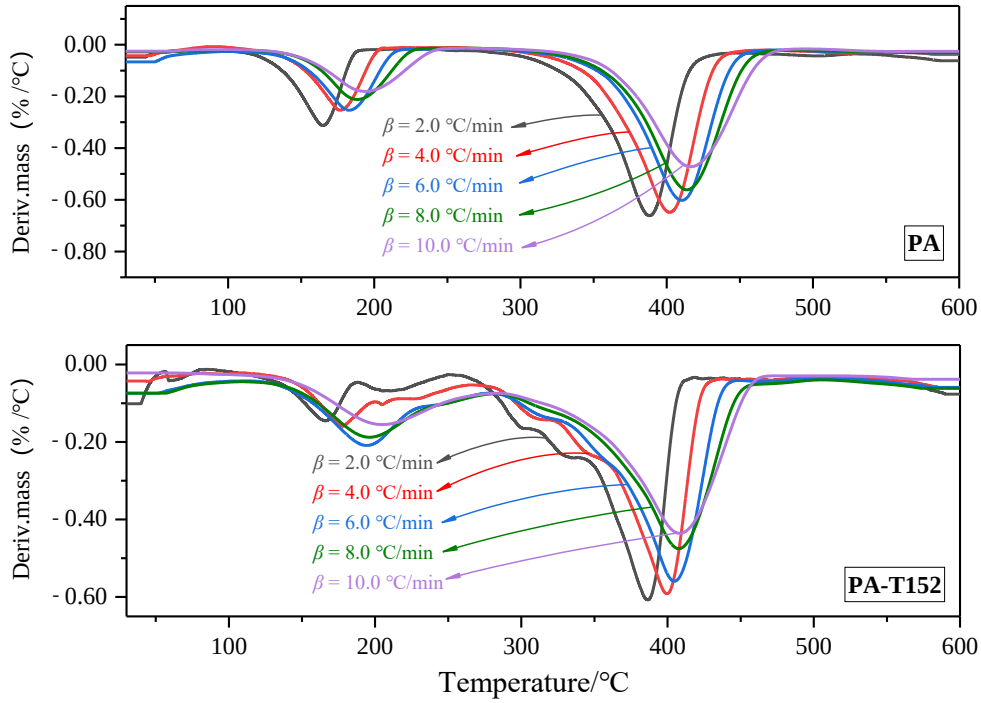

Figure 4. DTG curves of PA and PA-T152 at different β.

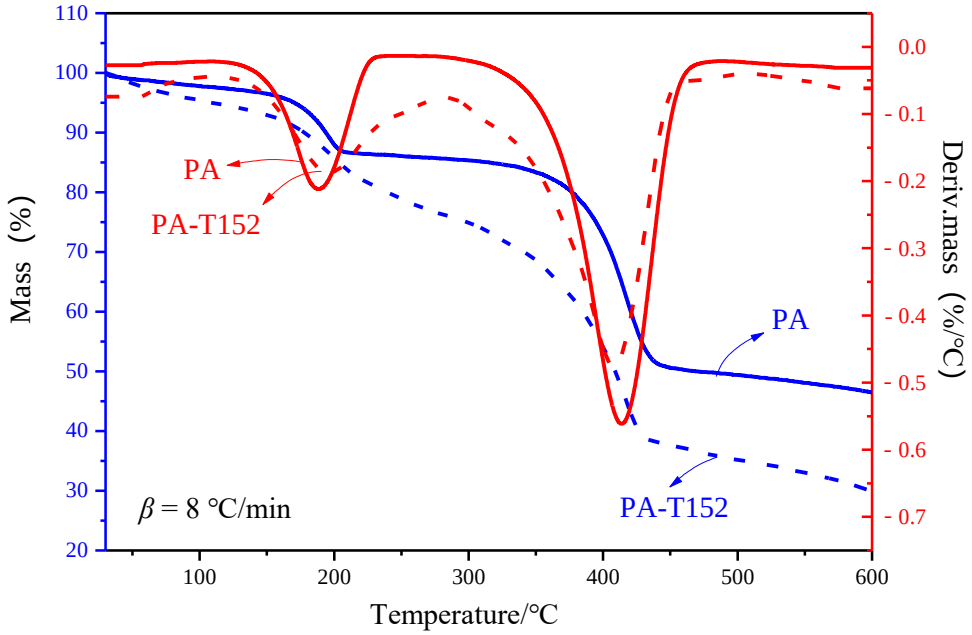

Figure 5. DTG curves of PA and PA-T152 at different β.

3.1.2. Heat Flow Analysis Results

The DSC non-isothermal experiments' results reveal PA's thermal decomposition process at β of 2.0, 4.0, 6.0, 8.0, and 10.0 °C/min. Experimental results demonstrate that the thermal decomposition of PA can be divided into two stages. The first stage is endothermic, and T_p is around 131–135 °C. The second stage is exothermic, and there are two exothermic peaks. Both T_{p1} and T_{p2} increased with the increase of β. The range of T_{p1} and T_{p2} ranged from 313 to 335 °C and 357 to 392 °C under the five β values. During the thermal decomposition of PA, the average ΔH value of different β is about 3322 J/g, the specific data are shown in Table 2

Table 2. E_a and R^2 values of PA-T152 were obtained through different methods.

Sample	**PA-T152**					
	E_a (kJ/mol)			**R^2**		
α	**Friedman**	**KAS**	**Starink**	**Friedman**	**KAS**	**Starink**
0.1	234.15	299.48	299.33	0.9631	0.9706	0.9708
0.2	145.85	183.71	184.04	0.9931	0.9886	0.9887
0.3	165.09	195.40	195.72	0.9892	0.9857	0.9859
0.4	167.26	193.35	193.69	0.9954	0.9896	0.9897
0.5	167.86	190.51	190.88	0.9935	0.9872	0.9873
0.6	163.75	184.23	184.64	0.9928	0.9850	0.9851
0.7	168.94	188.49	188.89	0.9907	0.9810	0.9812
0.8	178.74	196.05	196.44	0.9530	0.9443	0.9449
Average	173.95	203.90	204.20	0.9838	0.9790	0.9792

3.2. Calculation by Thermokinetic Equations

The E_a value of materials is an indispensable and essential reference when studying the thermal stability of composites if one is unable to accurately select the reaction mechanism function of the experimental sample. For kinetic analysis, different methods were used to calculate the E_a and pre-exponential factor of PA and PA-T152 to minimize errors caused by various factors. Pyrolysis kinetics calculations could be performed relatively accurately.

According to Equation (4), the Kissinger method was used for the linear fitting of PA and PA-T152, and the results were displayed in Figure 6. In Figure 6a, the slope of the line after fitting ln (β/T_p^2) and $1000/T_p$ is −24,338.38. Therefore, according to the slope

calculation, the E_a of PA is 202.35 kJ/mol. Similarly, the slope of the line after fitting in Figure 6b is −29,518.78, and the E_a value of PA-T152 can be calculated as 245.42 kJ/mol. Therefore, the values of the linear fit accuracy R^2 of the two lines are 0.9725 and 0.9624, respectively, which is close to 1, indicating that both sample models have a better fit.

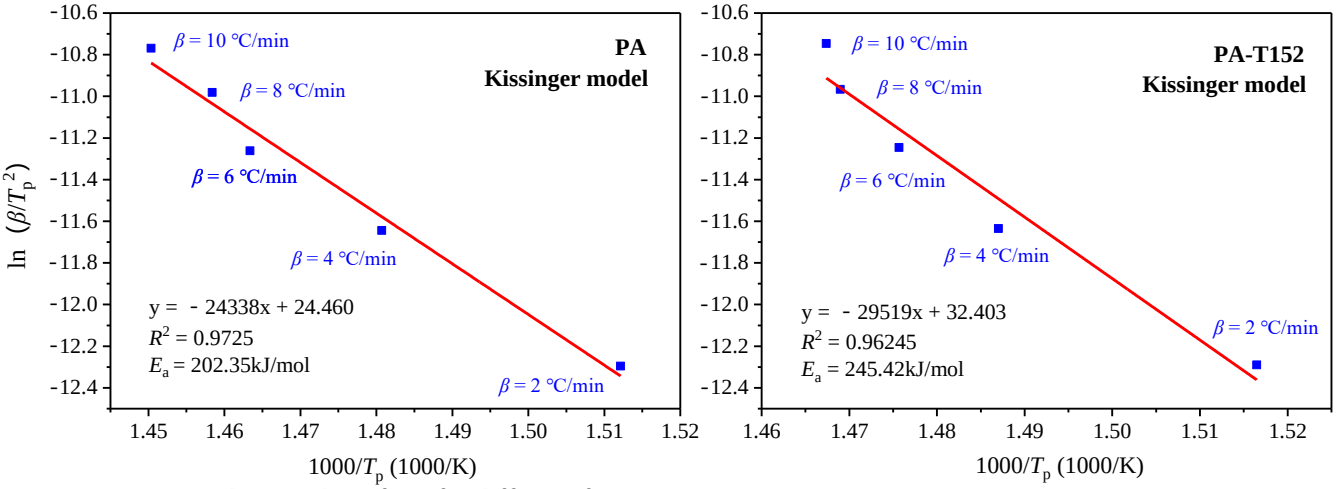

(a) The E_a value of PA for different β **(b)** The E_a value of PA-T152 for different β

Figure 6. E_a values of Kissinger method for different β in TGA experiments.

The E_a value is the maximum energy required for a material change. Therefore, the higher the value of E_a, the slower the thermal decomposition rate of the material. By comparing Figure 6a,b, the E_a value of PA-T152 (245.42 kJ/mol) is greater than that of pure PA (202.35 kJ/mol), indicating that the thermal stability of PA is improved after the addition of T152 emulsifier.

Different conversion methods (Friedman, KAS, FWO, Vyazovkin, and Starink) were used to calculate the thermokinetic parameters to ensure the reliability of the experimental results. The α value chosen for the calculation is between 0.05–0.99. However, the instability of the practical instrument and other factors lead to poor fitting accuracy when the α is less than 0.2 and larger than 0.8. Therefore, it is more instructive to select α fit at 0.2–0.8. The results of the calculations for PA and PA-T52 using the FWO method and the Vyazovkin method are shown in Figures 7 and 8, respectively. The results of calculating E_a and R^2 from TG curves of PA and PA-T152 using Friedman, KAS, and Starink methods are shown in Tables 3 and 4.

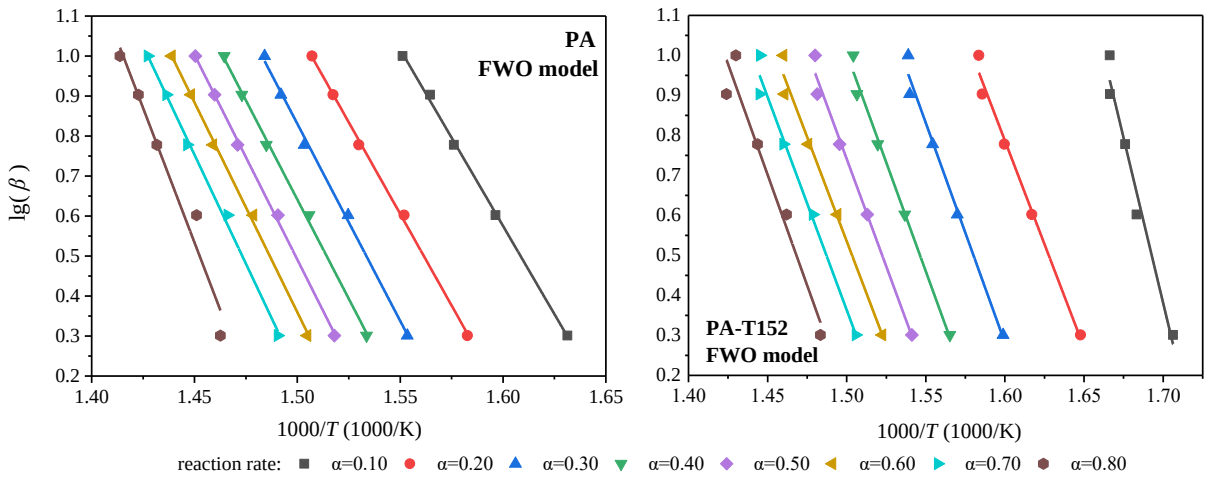

Figure 7. Calculation of E_a from TG curves for PA and PA-T152 using FWO model.

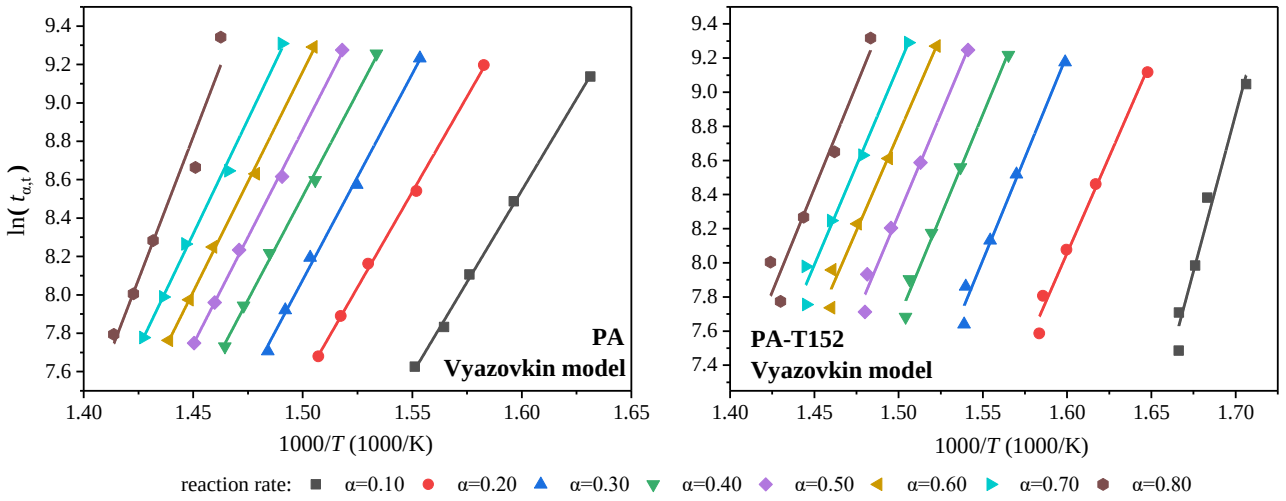

Figure 8. Calculation of E_a from TG curves for PA and PA-T152 using Vyazovkin model.

Table 3. Calorimetric data from dynamic scanning experiments of PA.

Sample		PA					
		Endothermic		Exothermic			
β (°C/min)	Mass (mg)	T_0 (°C)	T_p (°C)	T_0 (°C)	T_{p1} (°C)	T_{p2} (°C)	ΔH (/J g)
2.0		130–132	132–134	269–271	313–315	357–359	5284–5286
4.0		128–130	131–133	280–282	317–319	371–373	3712–3714
6.0	1.80 ± 0.5	130–132	132–134	283–285	327–329	378–380	2880–2882
8.0		130–132	133–135	286–288	333–335	385–387	2429–3431
10.0		128–130	132–133	299–301	332–334	390–392	2302–2304

Table 4. Thermogravimetric loss data for PA and PA-T152.

Sample	PA					
	E_a (kJ/mol)			R^2		
α	Friedman	KAS	Starink	Friedman	KAS	Starink
0.1	109.15	155.04	155.48	0.9934	0.9987	0.9987
0.2	122.07	161.02	161.48	0.9961	0.9986	0.9986
0.3	137.10	173.84	174.26	0.9970	0.9972	0.9972
0.4	140.29	174.90	175.33	0.9964	0.9978	0.9979
0.5	145.82	180.75	181.17	0.9962	0.9987	0.9987
0.6	151.14	185.46	185.87	0.9953	0.9983	0.9983
0.7	159.04	192.84	193.24	0.9931	0.9967	0.9967
0.8	203.88	240.66	240.90	0.9433	0.9595	0.9599
Average	146.06	183.06	183.47	0.9889	0.9932	0.9933

In Figure 7, the average E_a and R^2 of PA calculated by FWO are 184.40 kJ/mol and 0.9938, respectively; the average E_a and R^2 of PA-T152 calculated by FWO are 203.96 kJ/mol and 0.9810. In Figure 8, the average E_a and R^2 of PA calculated by Vyazovkin method are 183.96 kJ/mol and 0.9933, respectively; the average E_a and R^2 of PA-T152 calculated by Vyazovkin method are 204.55 kJ/mol and 0.9791. E_a and R^2 values of PA-T152 obtained through the other methods are shown in Tables 2 and 3.

The calculation results demonstrate that the E_a values obtained by the four equal conversion methods are similar. It indicates that the fitting results of these four methods are better than those of the Kissinger method. The average E_a calculated by the four methods is 183.72 kJ/mol. The average E_a of PA calculated by the Friedman method is 146.06 kJ/mol,

which is quite different from the average E_a calculated by other methods. The R^2 value of Friedman method is 0.9889, which is also smaller than the other four methods, indicating that the fitting accuracy of PA by Friedman method is not good enough. The parameters calculated by different thermokinetic methods are shown in Figure 9. Figure 9a is the E_a value obtained by the six calculation methods, and it can be found that the value obtained by the Friedman method is relatively small. Figure 9b shows the R^2 values obtained by the six calculation methods, and their linear fitting accuracy is very high. Therefore, other methods except Friedman are more suitable for calculating the E_a of PA and PA-T152.

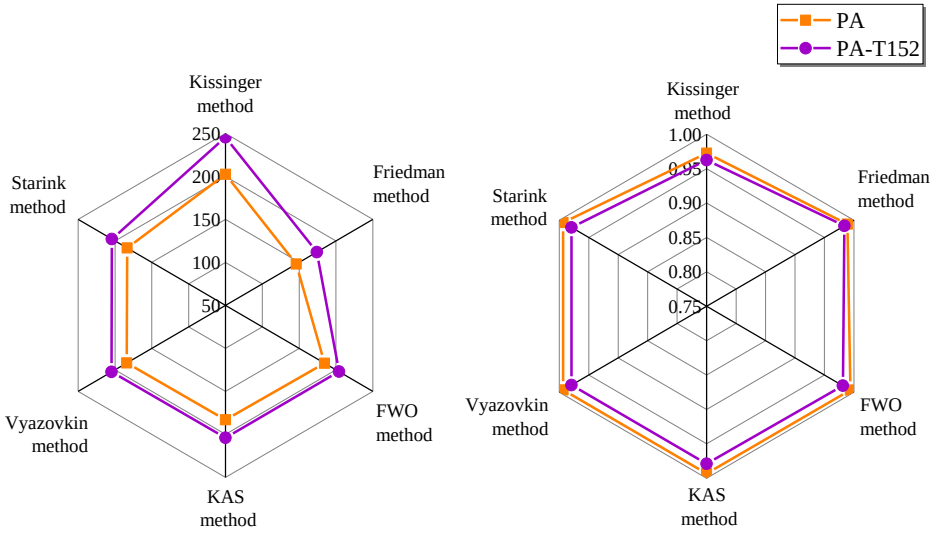

(a) The E_a value of PA and PA-T152 (b) The R^2 of PA and PA-T152

Figure 9. Radar plots of E_a values and R^2 calculated by different thermokinetic methods.

By the same calculation, the average E_a of PA-T152 obtained by the four thermokinetic calculation methods is 204.15 kJ/mol, which has increased compared with the average E_a of pure PA (183.72 kJ/mol). It has been proven that after adding the T152 emulsifier, the E_a of PA is improved, that is, the stability of PA-T152 becomes better.

3.3. FTIR Analysis

TG-FTIR analysis was used to infer the gas products escaping from PA and PA-T152 during thermal decomposition and thermogravimetry. Figure 10 shows three-dimensional FTIR images of PA and PA-T152 in the combustion process. The infrared spectra of the temperature corresponding to the peak weight loss of PA and PA-T152 at 427 °C is shown in Figure 11. The corresponding spectral absorption peak positions of the two samples are similar. The CO_2 absorption peaks of the two samples correspond at 2358 cm^{-1} [35], and the CO_2 absorption peaks in this wave number range are greatly enhanced when the pyrolysis temperature rises from 82–427 °C. The mass loss peak at 80–430 °C in the thermogravimetric curves of Figures 3 and 4 is related to the decomposition of the propellant to produce CO_2. The telescopic vibration peak near 1510 cm^{-1} is N=O, indicating that the nitro compounds in the fireworks propellant begin to decompose at this stage [36]. Unlike PA, an asymmetric shrinkage peak appeared in PA-T152 near 2932 cm^{-1} due to a change in CH_2 in T152 [37]. There was little difference between the prominent characteristic peaks of PA and PA-T152. However, the absorption peak intensity of PA after adding T152 was weaker than that of pure PA, indicating that the amount of carbon dioxide produced in the reaction process of PA-T152 was reduced. Because T152 inhibited PA thermal decomposition, the reaction's intensity was reduced.

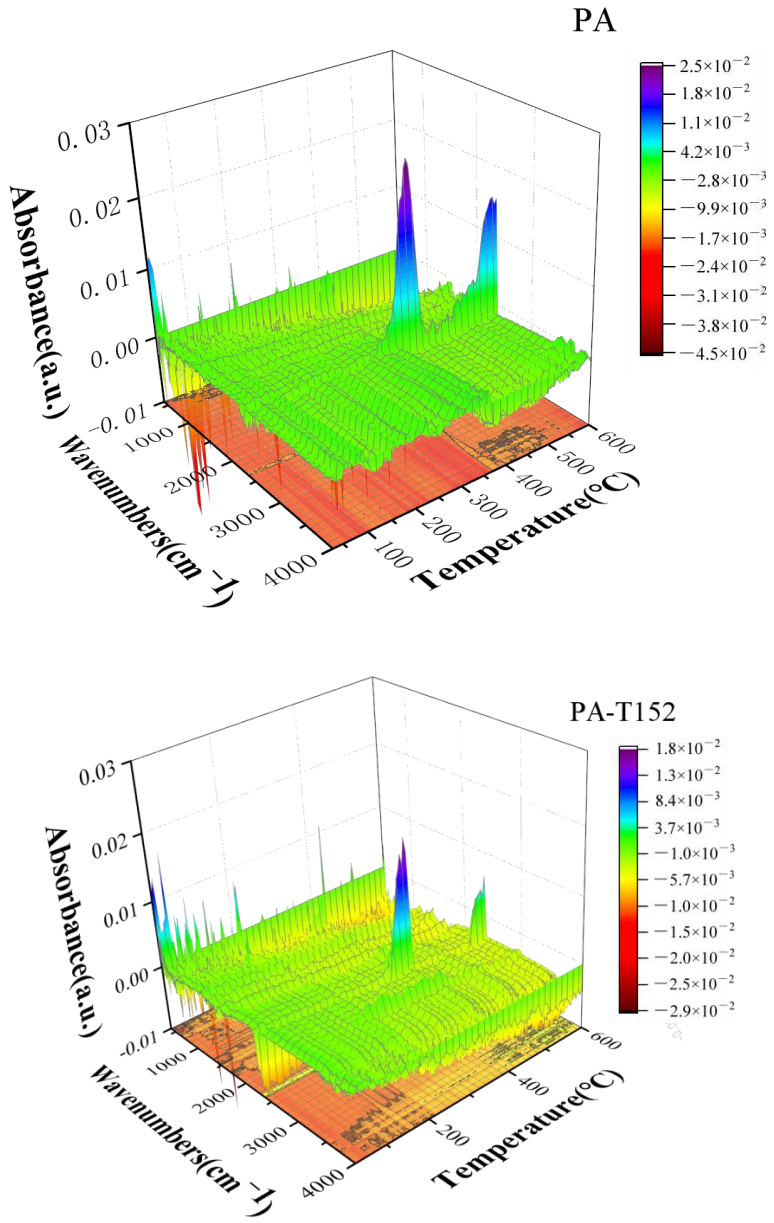

Figure 10. Three-dimensional TG-FTIR spectra of PA and PA-T152.

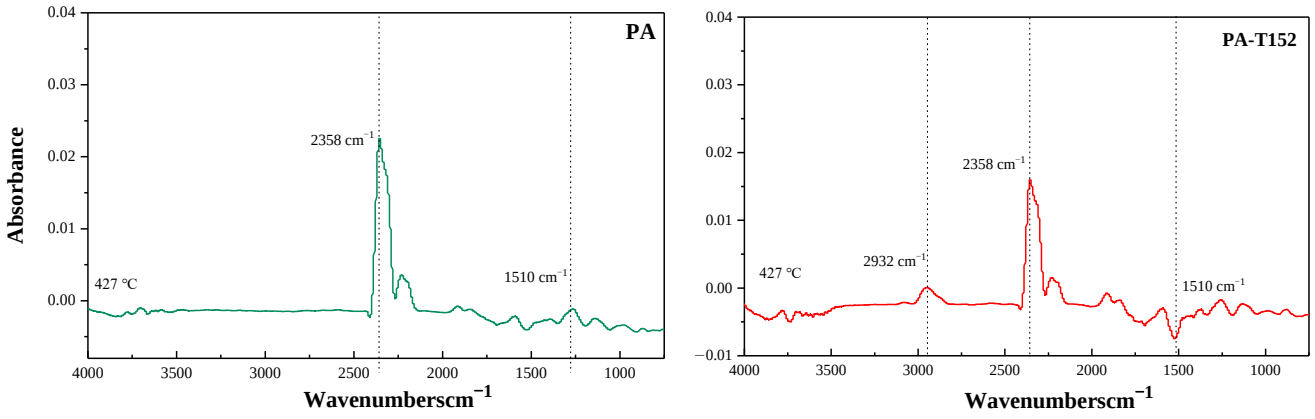

Figure 11. FTIR spectra of PA and PA-T152 at 427 °C.

4. Conclusions

The thermal decomposition process of PA and the effect of the T152 emulsifier on the thermal stability of PA were studied by TG-FTIR and DSC. The experimental results of TGA show that the mass-loss process of PA can be divided into two stages. Although the mass loss of PA is still divided into two stages after the addition of T152, the T_0 of the two stages is significantly higher than that of pure PA, which indicates that the addition of T152 reduces the decomposition rate of propellant and improves the thermal stability of PA. Furthermore, DSC results indicate that T_0 and T_p of PA are positively correlated with β in the exothermic stage. The average ΔH of PA is 3321.96 J/g.

Based on the thermokinetic parameters of TGA, the E_a values of PA and PA-T152 were calculated by Friedman, KAS, FWO, Vyazovkin, and Starink methods. The results indicate that KAS, FWO, Vyazovkin, and Starink methods best estimate the thermokinetic parameters of PA and PA-T152. The E_a values calculated by the four equal conversion methods are similar. The E_a of PA is 183.7 $\pm$ 0.8 kJ/mol, and PA-T152 is 204.2 $\pm$ 0.5 kJ/mol. The average E_a of PA-T152 is larger than that of pure PA, indicating that PA-T152 has higher thermal stability.

In addition, the FTIR results specify that the CO_2 absorption peaks of PA and PA-T152 were near 2358 cm^{-1}, and the CO_2 absorption peaks in the wave number range increased with the temperature rising and reached the maximum value at 430 °C. The N=O stretching vibration peaks near 1510 cm^{-1} indicate that nitro compounds begin to decompose. PA-T152 showed a contraction peak near 2932 cm^{-1}, indicating that CH_2 in T152 began to change. The characteristic peaks of PA and PA-T152 are similar, but the absorption peak intensity of PA after adding T152 is weaker than that of pure PA. Therefore, the amount of carbon dioxide produced by PA-T152 is reduced, and the reaction intensity is weaker than that of PA.

In summary, in PA storage and transportation, it is necessary to be alert to sudden and rapid ambient temperature increase, which makes it very easy for the PA self-reaction to cause violent spontaneous combustion or even an explosion in a short period. Therefore, mixing T152 with PA is beneficial to reduce the risk of thermal runaway of PA. Furthermore, the storage and transportation of PA should be carried out in a moisturizing state as much as possible to reduce the risk of thermal runaway. This study aids understanding of the thermal risk of pyrotechnic propellants. The data provided in this paper helps prevent thermal runaway accidents of firework propellants. However, the use of fireworks still needs further exploration to provide reference significance for practical application.

Author Contributions: Conceptualization, H.W.; validation and methodology, N.Y. and A.-C.H.; formal analysis and resources, Y.T.; writing—original draft preparation, H.W.; writing—review and editing, A.-C.H.; project administration and funding acquisition, J.-C.J. All authors have read and agreed to the published version of the manuscript.

Funding: This work was supported by the National Key Research Development Program of China (grant number 2021YFC3001203); National Natural Science Foundation of China (grant number 21927815); and Natural Science Foundation of the Jiangsu Higher Education Institutions of China (grant number 21KJB620003) for financial support.

Institutional Review Board Statement: Not applicable.

Informed Consent Statement: Not applicable.

Data Availability Statement: Not applicable.

Conflicts of Interest: The authors declare no conflict of interest.

References

1. Pang, N.; Gao, J.; Zhao, P.; Wang, Y.; Xu, Z.; Chai, F. The impact of fireworks control on air quality in four Northern Chinese cities during the Spring Festival. *Atmos. Environ.* **2021**, *244*, 117958. [CrossRef]
2. Ajith, S.; Sivapragasam, C.; Arumugaprabu, V. A review on hazards and their consequences in firework industries. *SN Appl. Sci.* **2018**, *1*, 120. [CrossRef]

3. Sun, Y.; Han, Z.; Du, Z.; Zengyi, L.; Cong, X. Preparation and performance of environmental friendly Sulphur-Free propellant for fireworks. *Appl. Therm. Eng.* **2017**, *126*, 987–996. [CrossRef]
4. Lin, W.-C.; Chen, W.-C.; Shu, C.-M. Thermal stability evaluation of multiple tubes of fireworks by calorimetry approaches. *J. Therm. Anal. Calorim.* **2019**, *138*, 2883–2890. [CrossRef]
5. Wu, H.; Jiang, J.-C.; Huang, A.-C.; Tang, Y.; Liu, Y.-C.; Zhai, J.; Shu, C.-M.; Xing, Z.-X. Effect of emulsifiers on the thermal stability of firework propellants. *J. Therm. Anal. Calorim.* **2022**, 1–9. [CrossRef]
6. Zhao, J.; Cheng, Y.-C.; Hou, H.-Y.; Chen, W. Applications of intrinsic safety characteristic parameters of propellant dust: Commercial multi-tube pyrotechnic hazard assessment. *J. Loss Prev. Process Ind.* **2021**, *69*, 104381. [CrossRef]
7. Ye, W.-X. Investigation and Identification of Fire Caused by Setting off Fireworks. *Procedia Eng.* **2016**, *135*, 427–430. [CrossRef]
8. Wang, X.; Zhou, L.; Zhu, S.-Q.; Zheng, H.; Ma, Y.; Liu, Y.; Jia, C.; Zhou, C.-L.; Bie, L.; Zhang, G. Modes of Occurrence of Chromium and Their Thermal Stability in Low-Rank Coal Pyrolysis. *Processes* **2021**, *10*, 15. [CrossRef]
9. Cao, C.-R.; Chen, W.-C.; Shu, C.-M. Prediction and assessment of fly-up type of fireworks by thermokinetics model. *J. Therm. Anal. Calorim.* **2020**, *142*, 927–936. [CrossRef]
10. Tafu, N.N.; Jideani, V.A. Characterization of Novel Solid Dispersions of Moringa oleifera Leaf Powder Using Thermo-Analytical Techniques. *Processes* **2021**, *9*, 2230. [CrossRef]
11. Ren, S.-J.; Wang, C.-P.; Xiao, Y.; Deng, J.; Tian, Y.; Song, J.; Cheng, X.-J.; Sun, G. Thermal properties of coal during low temperature oxidation using a grey correlation method. *Fuel* **2020**, *260*, 116287. [CrossRef]
12. Zheng, H.; Mao, L.; Yang, J.; Zhang, C.; Miao, S.; Gao, Y. Effect of Oil Content and Emulsifier Type on the Properties and Antioxidant Activity of Sea Buckthorn Oil-in-Water Emulsions. *J. Food Qual.* **2020**, *2020*, 1–8. [CrossRef]
13. Drapala, K.P.; Auty, M.A.E.; Mulvihill, D.M.; O'Mahony, J.A. Influence of emulsifier type on the spray-drying properties of model infant formula emulsions. *Food Hydrocoll.* **2017**, *69*, 56–66. [CrossRef]
14. Ouqi, N. Synthesis of Alkylol Amine Emulsifiers and Their Application in Emulsion Explosive. *Explos. Mater.* **2013**, *4*, 6–9.
15. Zhao, Z.; Yue, J.; Ji, X.; Nian, M.; Kang, K.; Qiao, H.; Zheng, X. Research progress in biological activities of succinimide derivatives. *Bioorg. Chem.* **2020**, *108*, 104557. [CrossRef]
16. Ruffell, J.; Farmer, T.J.; Macquarrie, D.J.; Stark, M.S. The Autoxidation of Alkenyl Succinimides—Mimics for Polyisobutenyl Succinimide Dispersants. *Ind. Eng. Chem. Res.* **2019**, *58*, 19649–19660. [CrossRef]
17. Huang, A.-C.; Huang, C.-F.; Xing, Z.-X.; Jiang, J.-C.; Shu, C.-M. Thermal hazard assessment of the thermal stability of acne cosmeceutical therapy using advanced calorimetry technology. *Process Saf. Environ. Prot.* **2019**, *131*, 197–204. [CrossRef]
18. Kaljuvee, T.; Štubňa, I.; Húlan, T.; Uibu, M.; Einard, M.; Traksmaa, R.; Viljus, M.; Jefimova, J.; Trikkel, A.J.P. Thermal Behavior of Ceramic Bodies Based on Estonian Clay from the Arumetsa Deposit with Oil Shale Ash and Clinker Dust Additives. *Processes* **2021**, *10*, 46. [CrossRef]
19. Martinez-Gómez, C.; Rangel-Vázquez, I.; Zarraga, R.; del Ángel, G.; Ruíz-Camacho, B.; Tzompantzi, F.; Vidal-Robles, E.; Pérez-Larios, A. Photodegradation and Mineralization of Phenol Using TiO_2Coated γ-Al_2O_3: Effect of Thermic Treatment. *Processes* **2022**, *10*, 1186. [CrossRef]
20. Anucha, C.B.; Bacaksız, E.; Stathopoulos, V.N.; Pandis, P.K.; Argirusis, C.; Andreouli, C.; Tatoudi, Z.; Altin, I. Molybdenum Modified Sol–Gel Synthesized TiO_2 for the Photocatalytic Degradation of Carbamazepine under UV Irradiation. *Processes* **2022**, *10*, 1113. [CrossRef]
21. Zhou, H.-L.; Jiang, J.-C.; Huang, A.-C.; Tang, Y.; Zhang, Y.; Huang, C.-F.; Liu, S.; Shu, C.-M. Calorimetric evaluation of thermal stability and runaway hazard based on thermokinetic parameters of O,O–dimethyl phosphoramidothioate. *J. Loss Prev. Process Ind.* **2022**, *75*, 104697. [CrossRef]
22. Yang, Y.-P.; Huang, A.-C.; Tang, Y.; Liu, Y.-C.; Wu, Z.-h.; Zhou, H.-L.; Li, Z.-P.; Shu, C.-M.; Jiang, J.-C.; Xing, Z.-X. Thermal Stability Analysis of Lithium-Ion Battery Electrolytes Based on Lithium Bis(trifluoromethanesulfonyl)imide-Lithium Difluoro(oxalato)Borate Dual-Salt. *Polymers* **2021**, *13*, 707. [CrossRef] [PubMed]
23. Li, Z.-P.; Jiang, J.-C.; Huang, A.-C.; Tang, Y.; Miao, C.-F.; Zhai, J.; Huang, C.-F.; Xing, Z.-X.; Shu, C.-M. Thermal hazard evaluation on spontaneous combustion characteristics of nitrocellulose solution under different atmospheric conditions. *Sci. Rep.* **2021**, *11*, 24053. [CrossRef] [PubMed]
24. Jia, G. Combustion Characteristics and Kinetic Analysis of Biomass Pellet Fuel Using Thermogravimetric Analysis. *Processes* **2021**, *9*, 868. [CrossRef]
25. Yang, N.; Jiang, J.-C.; Huang, A.-C.; Tang, Y.; Li, Z.-P.; Cui, J.; Shu, C.-M.; Xing, Z. Thermokinetic model-based experimental and numerical investigation of the thermal hazards of nitrification waste. *J. Loss Prev. Process Ind.* **2022**, *79*, 104836. [CrossRef]
26. Huang, A.-C.; Li, Z.-P.; Liu, Y.-C.; Tang, Y.; Huang, C.-F.; Shu, C.-M.; Xing, Z.-X.; Jiang, J.-C. Essential hazard and process safety assessment of para-toluene sulfonic acid through calorimetry and advanced thermokinetics. *J. Loss Prev. Process Ind.* **2021**, *72*, 104558. [CrossRef]
27. Liu, Y.-C.; Jiang, J.-C.; Huang, A.-C.; Tang, Y.; Yang, Y.-P.; Zhou, H.-L.; Zhai, J.; Xing, Z.; Huang, C.-F.; Shu, C.-M. Hazard assessment of the thermal stability of nitrification by-products by using an advanced kinetic model. *Process Saf. Environ. Prot.* **2022**, *160*, 91–101. [CrossRef]
28. Friedman, H.L. Kinetics of thermal degradation of char-forming plastics from thermogravimetry. Application to a phenolic plastic. *J. Polym. Sci. Part C Polym. Lett.* **2007**, *6*, 183–195. [CrossRef]

29. Yao, C.; Liu, Y.-C.; Wu, J.; Tang, Y.; Zhai, J.; Shu, C.-M.; Jiang, J.-C.; Xing, Z.-X.; Huang, C.-F.; Huang, A.-C. Thermal Stability Determination of Propylene Glycol Sodium Alginate and Ammonium Sulfate with Calorimetry Technology. *Processes* **2022**, *10*, 1177. [CrossRef]
30. Xie, L.; Jiang, J.-C.; Huang, A.-C.; Tang, Y.; Liu, Y.-C.; Zhou, H.-L.; Xing, Z. Calorimetric Evaluation of Thermal Stability of Organic Liquid Hydrogen Storage Materials and Metal Oxide Additives. *Energies* **2022**, *15*, 2236. [CrossRef]
31. Huang, A.-C.; Liao, F.C.; Huang, C.-F.; Tang, Y.; Zhang, Y.; Shu, C.-M.; Xing, Z.-X.; Jiang, J.-C.; Hsieh, W.-Y. Calorimetric approach to establishing thermokinetics for cosmeceutical benzoyl peroxides containing metal ions. *J. Therm. Anal. Calorim.* **2021**, *144*, 373–382. [CrossRef]
32. Vyazovkin, S. Kissinger Method in Kinetics of Materials: Things to Beware and Be Aware of. *Molecules* **2020**, *25*, 2813. [CrossRef] [PubMed]
33. Chen, F.; Dong, X.; Tang, Y.; Huang, A.-C.; Zhang, M.; Kang, Q.; Shu, Z.-J.; Xing, Z. Thermal Characteristic Analysis of Sodium in Diluted Oxygen via Thermogravimetric Approach. *Processes* **2022**, *10*, 704. [CrossRef]
34. Zhang, C.; Jiang, J.-C.; Huang, A.-C.; Tang, Y.; Xie, L.; Zhai, J.; Xing, Z. A novel multifunctional additive strategy improves the cycling stability and thermal stability of SiO/C anode Li-ion batteries. *Process Saf. Environ. Prot.* **2022**, *164*, 555–565. [CrossRef]
35. Chen, Y.; Wang, L.; Zhao, M.; Ma, H.; Chen, D.; Zhang, Y.; Zhou, J. Comparative Study on the Pyrolysis Behaviors of Pine Cone and Pretreated Pine Cone by Using TGA–FTIR and Pyrolysis-GC/MS. *ACS Omega* **2021**, *6*, 3490–3498. [CrossRef] [PubMed]
36. Guo, Y.; Zhao, N.; Zhang, T.; Gong, H.; Ma, H.-X.; An, T.; Zhao, F.; Hu, R.-Z. Compatibility and thermal decomposition mechanism of nitrocellulose/Cr_2O_3 nanoparticles studied using DSC and TG-FTIR. *RSC Adv.* **2019**, *9*, 3927–3937. [CrossRef]
37. Wu, D.; Zhang, W.; Fu, B.; Hu, G. Chemical structure and gas products of different rank coals during pyrolysis. *J. Therm. Anal. Calorim.* **2018**, *136*, 2017–2031. [CrossRef]